iScience

CellPress
OPEN ACCESS

Article

Low-temperature resin embedding of the whole brain for various precise structures dissection

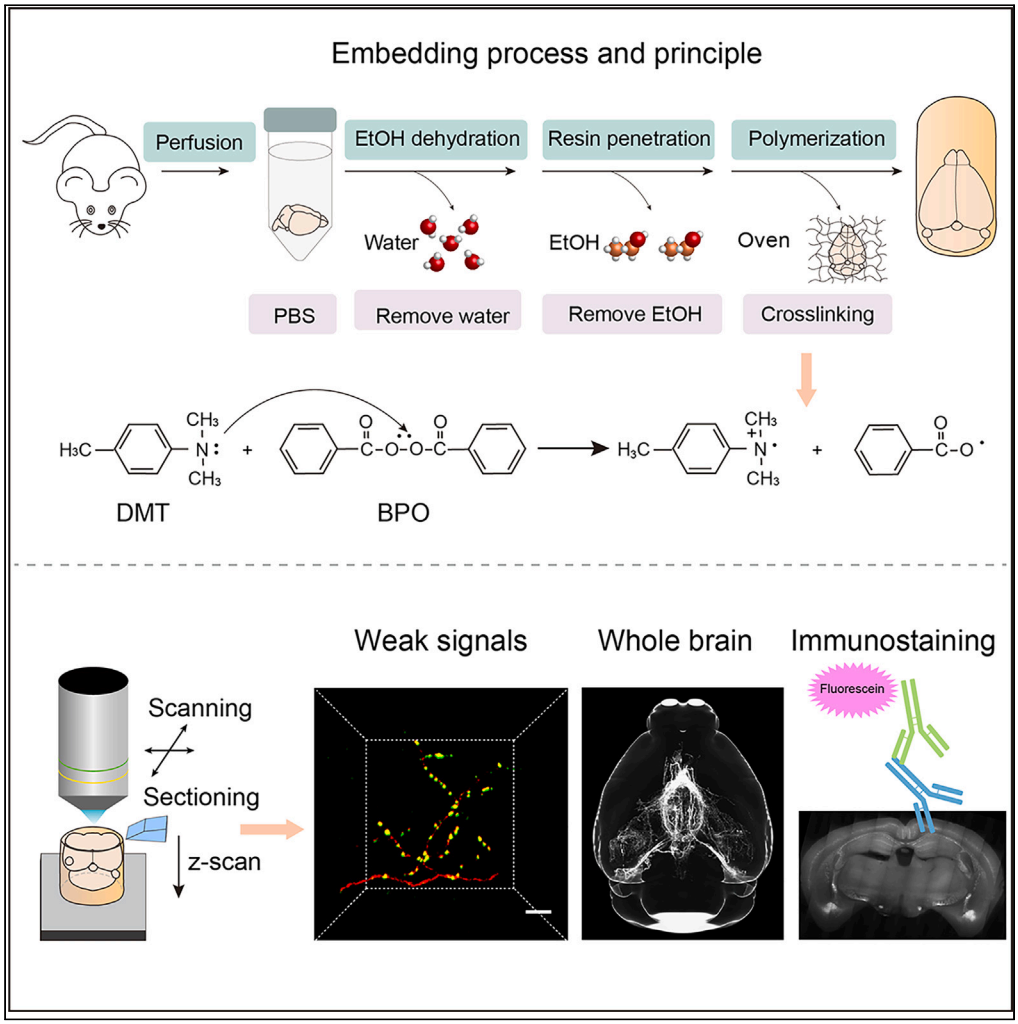

Jiaojiao Tian, Yingying Chen, Tao Jiang, Xueyan Jia, Hui Gong, Xiangning Li

lixiangning@mail.hust.edu.cn

Highlights

A resin embedding method to polymerize whole brains at low temperature

The optimized method maintained weak signals of precise structures

The HM20-T method was suitable for various fluorescent proteins or dyes

The immunoreactivity of bio-tissues was preserved after embedding

Tian et al., iScience 26, 106705
May 19, 2023
https://doi.org/10.1016/j.isci.2023.106705

iScience

CellPress
OPEN ACCESS

Article

Low-temperature resin embedding of the whole brain for various precise structures dissection

Jiaojiao Tian,[1,4] Yingying Chen,[1] Tao Jiang,[3] Xueyan Jia,[3] Hui Gong,[1,3] and Xiangning Li[1,2,3,5,*]

SUMMARY

Resin embedding combined with ultra-thin sectioning has been widely used in microscopic and electron imaging to acquire precise structural information of biological tissues. However, the existing embedding method was detrimental to quenchable fluorescent signals of precise structures and pH-insensitive fluorescent dyes. Here, we developed a low-temperature chemical polymerization method named HM20-T to maintain weak signals of various precise structures and to decrease background fluorescence. The fluorescence preservation ratio of green fluorescent protein (GFP) tagged presynaptic elements and tdTomato labeled axons doubled. The HM20-T method was suitable for a variety of fluorescent dyes, such as DyLight 488 conjugated Lycopersicon esculentum lectin. Moreover, the brains also retained immunoreactivity after embedding. In summary, the HM20-T method was suitable for the characterization of multi-color labeled precise structures, which would contribute to the acquisition of complete morphology of various biological tissues and to the investigation of composition and circuit connection in the whole brain.

INTRODUCTION

The brain is the most complex biological organ in higher animals, containing various types of neurons, glial cells, and blood vessels. Dissection of complete structures in the nervous system is the cornerstone of understanding the organization and functions of the brain. With the development in tracer and imaging technologies, the whole-brain view or the ultrastructure information has been investigated in different models. The neural circuits consist of different types of neurons, which transmit the information by long-range axons to their targeting areas in the whole brain. Axons have multiple orders of branches with different diameters.[1,2] With viral tracing, different types of fluorescent proteins and fluorescent dyes were used to label axons and other precise structures with various fluorescence intensity. Adeno-associated virus (AAV)[3] or rotavirus[4] carrying fluorescent proteins and neural tracer dyes, such as green fluorescence protein (GFP),[5,6] red fluorescence protein (RFP), blue fluorescence protein (BFP), cholera toxin subunit (CTB),[5] Fluoro-Gold,[7] and phaseolus vulgaris agglutinin (PHAL),[8] are used for precise structures of output and input neural circuits studies. Moreover, vascular fine structures were marked by fluorescence dyes through caudal vein or cardiac perfusion, such as lectin series[9] and fluorescein isothiocyanate (FITC).[10] In addition, staining and observation of pathological features such as amyloid-β plaque labeled by immunostaining or fluorescein probe contribute to understanding the pathogenesis of Alzheimer's disease (AD).[11] Therefore, to better understand the interaction of the various components of the brain, we should acquire the fluorescent signals of multiple fine structures with sub-micron resolution.

Resin embedding combined with ultra-thin sectioning of fluorescent micro-optical section tomography (fMOST) has been widely used to acquire information of fine structures of biological tissues.[12–15] HM20 resin embedding is suitable for long-term imaging of fine structures, but the polymerization temperature of the existing embedding methods was mostly higher than 50°C.[16] In embedding procedures, fluorescence was significantly quenched, and the fluorescence of GFP could be recovered by adjusting the pH value, but it was difficult to recover the fluorescence of fine structures and some pH-insensitive fluorophores after embedding. In addition, high polymerization temperature caused increased autofluorescence of biological tissues,[17,18] which limited application of such methods in fine structures with weak signals. Here, we developed a low-temperature polymerization method, which could retain multi-color labeled precise signals while keeping background fluorescence low.

[1]Britton Chance Center and MoE Key Laboratory for Biomedical Photonics, Wuhan National Laboratory for Optoelectronics, Huazhong University of Science and Technology, Wuhan 430074, China

[2]Key Laboratory of Biomedical Engineering of Hainan Province, School of Biomedical Engineering, Hainan University, Haikou 570228, China

[3]Research Unit of Multimodal Cross Scale Neural Signal Detection and Imaging, Chinese Academy of Medical Sciences, HUST-Suzhou Institute for Brainmatics, JITRI, Suzhou 215125, China

[4]Department of Clinical Laboratory, The First Affiliated Hospital of Zhengzhou University, Zhengzhou 450052, Henan, China

[5]Lead contact

*Correspondence: lixiangning@mail.hust.edu.cn

https://doi.org/10.1016/j.isci.2023.106705

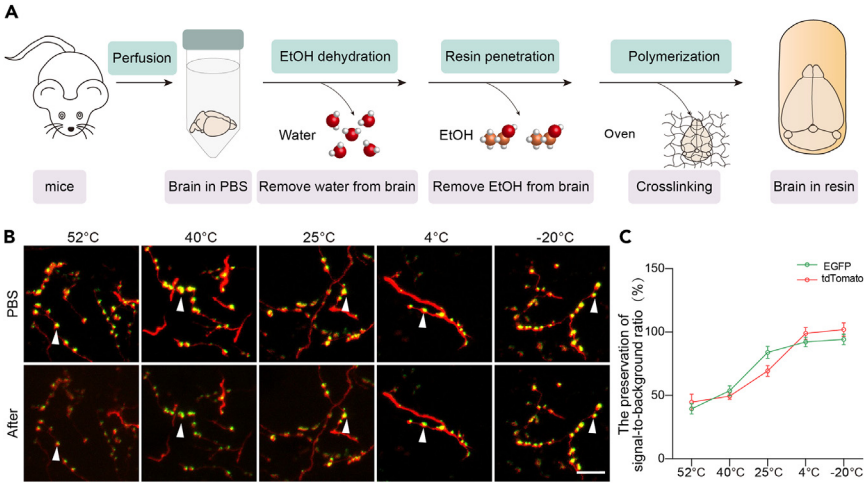

Figure 1. The factors affecting on fluorescent signals of precise structures

(A) Pipeline for resin embedding method.

(B) The effect of different temperatures on the fluorescent signals of SypEGFP and tdTomato. The white arrows showed the comparison of the same signal before and after different temperatures treatment.

(C) Quantitative analysis of the preservation ratio of signal-to-background ratio at different temperatures. (EGFP: 52°C, n = 3; 40°C, n = 5; 25°C, n = 3; 4°C, n = 3; −20°C, n = 3. tdTomato: 52°C, n = 3; 40°C, n = 5; 25°C, n = 3; 4°C, n = 4; −20°C, n = 4. Each n value represents an independent experiment). Data presented as mean ± SEM. Raw data were shown in Table S1. Scale bar: (B) 10 μm.

We chose chemical polymerization method with low activation energy for embedding to reduce the polymerization temperature needed. However, this method had not yet been performed on large-volume tissue, not even on the whole mouse brain because it was difficult to maintain the integrity of large tissue samples.[19,20] In this study, we screened a variety of methods for the most suitable temperature for polymerization and chose the chemical polymerization method for its low polymerization temperature. We used a polymerization accelerator and screened for the optimal concentration, which could embed the whole brain stably in two days, improving the signal-to-background ratio. In addition, by using this embedding method, we were able to visualize the fine structures of boutons, amyloid-β plaque, and blood vessels. Moreover, this optimized method also was capable of immunoreactivity. Therefore, the embedding method could satisfy the requirement of simultaneous acquisition of multiple fine structures information of the complete biological tissue in neurobiology research and assist the comprehensive and accurate analysis of the structure and function of the nervous system.

RESULTS

Low-temperature increased signal-to-background ratio of precise structures

Resin embedding steps included perfusion, rinse, alcohol dehydration, resin penetration, and polymerization (Figure 1A). After perfusion, the brains were post-fixed, rinsed, dehydrated with different concentrations of alcohol to remove water, infiltrated into the resin with different concentrations to replace the alcohol, and finally polymerized in an oven. Based on previous research, we found that the temperature during sample preparation affected fluorescence intensity, especially of the signals of precise structures. However, the existing HM20 resin embedding methods used heating polymerization method with the polymerization temperature around 52°C, which weakens the signal of boutons labeled by GFP or RFP.

Therefore, to explore the effect of different polymerization temperatures on the fluorescent signals of precise structure, we tested five groups of temperatures (52°C, 40°C, 25°C, 4°C, and −20°C). We injected the AAV2/9-hSyn-flex-tdTomato-T2A-synaptophysin-EGFP-WPRE-pA virus into mice to label weak signals of presynaptic elements with EGFP and axon fibers with tdTomato. The samples were sliced to 70 μm, and adjacent brain slices were imaged before processing. Then, the brain slices were placed in different temperatures for 48 h. Last, brain slices were taken out and imaged at the same position with the same parameters. As shown in Figure 1B, the presynaptic elements and tdTomato fluorescent proteins were severely quenched and the background fluorescent signals could were significantly increased in the 52°C and

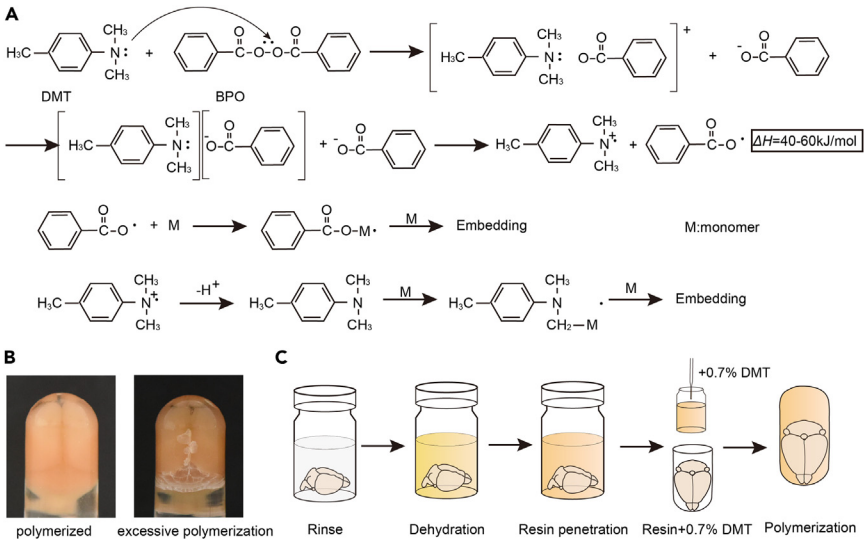

Figure 2. Established HM20-T resin embedding method

(A) Principle of redox reactions system. The main principle of this reaction was the reaction of DMT with BPO, which promoted the release of free radicals from BPO and then initiated the polymerization of monomers and crosslinkers.

(B) Polymerization state of the resin embedding sample at different concentrations of DMT and BPO.

(C) Schematic diagram illustrating the procedure for whole-brain resin embedding. We added 0.7% DMT in polymer solution and embedded samples at −20°C.

40°C groups. In the 25°C groups, the fluorescent signals of the presynaptic elements were well preserved, but the signals of axons were indistinguishable from the background. However, in the 4°C or −20°C groups, the SypEGFP and axons signals were still visible, and the level of background fluorescence were not changed after treatment. In the 52°C, 40°C, 25°C, 4°C, and −20°C groups, the signal-to-background ratio of the SypEGFP groups were 39.47 ± 4.00%, 53.72 ± 3.86%, 83.89 ± 4.80%, 92.15 ± 3.79%, and 94.13 ± 4.21%, respectively (Figure 1C and Table S1). The signal-to-background ratio in the tdTomato groups were 44.73 ± 6.32%, 49.49 ± 2.60%, 69.34 ± 4.29%, 98.89 ± 4.67%, and 101.96 ± 5.23%, respectively (Figure 1C and Table S1). In conclusion, lower polymerization temperature during the resin embedding preserved more fluorescent signals of GFP and tdTomato. The polymerization temperature was preferably 4°C or −20°C.

Established low-temperature resin embedding method

To reduce the polymerization temperature to 4°C or −20°C, we chose chemical polymerization instead of heat polymerization. In previous resin embedding methods, benzoyl peroxide (BPO) and N, N-Dimethylaniline (DMA) were used as initiator and accelerator (called redox system) and polymerization temperatures at −20°C–4°C.[20–22] Considering the volume of the whole brain, the chemical polymerization method was unsuitable for embedding the whole brain or larger tissues during two days. Here, we tried to replace DMA with N, N-Dimethyl-*p*-toluidine (DMT), which has lower activation energy, higher the reaction rate, and shorter induction period (Table S2).[23,24] DMT combined with BPO is expected to embed the whole brain samples at low temperature. We also tested polymerization effect at −20°C according to most of the studies.

Moreover, the ratio of initiator and accelerator for resin polymerization was an important factor affecting aggregation. With BPO as the initiator and DMT as the accelerator to release free radicals, the reaction of resin monomer and crosslinker could be initiated during polymerization (Figure 2A). Therefore, we tested the polymerization effect with different concentrations of BPO and DMT at −20°C (Table 1). When the concentration of BPO was over 1%, the resin was over-polymerized (Figure 2B). When BPO was 0.8% and DMT was over 0.5%, the resin was also over-polymerized (Figure 2B). When BPO was under 0.6%, the resin could not polymerize in two days. As shown in Table 1, the best concentration of BPO was 0.6%.

Moreover, to obtain the datasets with high resolution, especially on the z axis, we sectioned the sample with a diamond knife.[12,14] During whole brain imaging, the samples were continuously immersed in water

Table 1. Screening the concentration of DMT and BPO

BPO DMT	0.40%	0.60%	0.80%	1%	1.20%
0.40%	×	×	✓	✓	#
0.50%	×	✓	✓	#	N/A
0.60%	×	✓	#	#	N/A
0.70%	×	✓	#	#	N/A
0.80%	×	✓	#	#	N/A

The optimal concentration of DMT and BPO (× represents the resin un-polymerization during two days. ✓ represents the resin polymerization during two days. # represents the resin over-polymerization. N/A represents that the experiment was not performed.).

environment for more than ten days, so we needed to keep the embedded samples with consistent hardness over 15 consecutive days. When the concentration of DMT was 0.5% or 0.6%, the resin hardness was too low to meet the requirement of whole-brain imaging for long-time sectioning (Table 2). The 0.6% BPO combined with 0.7% DMT was the optimal concentration for whole-brain embedding and could keep the structure over ten days. We used this concentration to conduct different sets of experiments with more than a hundred brain samples. The success rate of embedding was over 98%. These results showed that our optimized method called HM20-T was stable and reproducible. In conclusion, the steps of the HM20-T embedding method included phosphate buffered saline (PBS) rinsing, ethanol dehydration, resin penetration, and resin polymerization containing 0.7% DMT at −20°C (Figure 2C).

Precise structures labeled by fluorescent protein were well preserved in HM20-T method

To confirm whether the HM20-T embedding method was suitable for brain samples with GFP fluorescent signals, we quantified the preservation rate of fluorescence and compared the number of labeled presynaptic elements before and after embedding (Figure 3A). Compared with the HM20 method, our method had increased the fluorescence preservation rate from 38.61 ± 2.44% to 82.54 ± 1.41% (unpaired t-test, $p < 0.0001$) (Figure 3B and Table S3), and the presynaptic elements preservation rate increased from 52.82 ± 2.30% to 95.52 ± 0.61% (unpaired t-test, $p < 0.0001$) (Figure 3C and Table S4). These results revealed that presynaptic elements signals labeled by EGFP could be well preserved in the HM20-T method.

To test the effect on RFP fluorescent proteins, we quantitatively analyzed the preservation of RFP fluorescent proteins using the HM20-T method. With VIP-ires-Cre;Ai14 mice expressing tdTomato in the VIP positive neurons, we tested the fluorescence preservation rate of different embedding methods (Figures 3D–3H). The result showed that the HM20-T method could significantly improve the signal-to-background ratio of fluorescent signals (Figures 3E and 3F, and Table S5), whereas the preservation of tdTomato increased by 1-fold (from 38.61 ± 2.44% to 83.09 ± 1.10%, Figures 3E and 3H, and Table S6). The precise structures, including thin axons and boutons, were well preserved after HM20-T embedding (Figure 3G). These results demonstrated that the HM20-T method was suitable for imaging precise structures labeled by multiple fluorescent proteins simultaneously, including both EGFP and tdTomato.

In addition, we tested commonly used YFP and mRuby fluorescent proteins using HM20-T method. As shown in Figure S1, this method well preserved fluorescent signals and precise structures. Combined with Thy-YFP mice and fMOST system, we could observe the morphology of neurons and axons in different coronal regions

Table 2. Water resistance test of DMT in different concentrations

Time DMT	1 day	3 days	5 days	10 days	15 days
0.5%	78	76	76	74	74
0.6%	80	80	78	78	78
0.7%	86	86	84	84	84
0.8%	86	86	86	84	84

Detection of hardness in water with different concentrations of DMT during 15 days. With an increase of DMT concentration, the higher hardness of the resin, the better the water resistance.

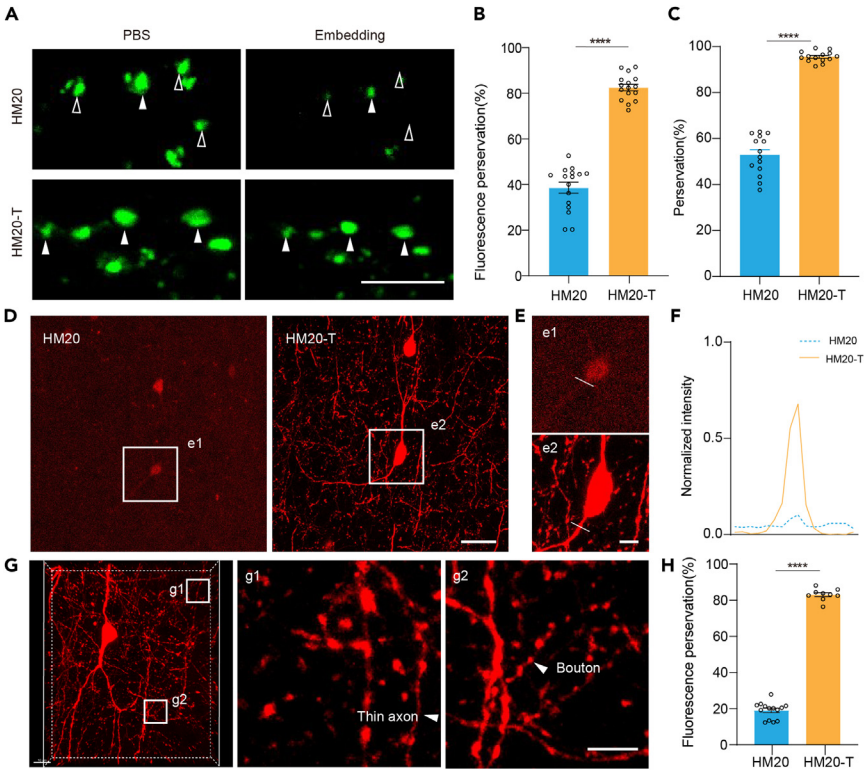

Figure 3. The fine structures labeled by EGFP and tdTomato could be well preserved in the HM20-T method

(A) Presynaptic elements were embedded in HM20 and HM20-T methods. The solid white arrow represented that the presynaptic elements were preserved after embedding. The white hollow arrow represented that the presynaptic elements were quenched after embedding.

(B) Comparison of fluorescence preservation in HM20 and HM20-T embedding methods. (n =16 independent experiments for each group). Data presented as mean ± SEM. Statistical analysis was performed by unpaired t-test, ****$p < 0.0001$.

(C) Quantitative analysis of presynaptic elements preservation of virus-labeled samples before and after embedding (n =14 independent experiments for each group). Data presented as mean ± SEM. Statistical analysis was performed by unpaired t-test, ****$p < 0.0001$.

(D) Fluorescence comparison of tdTomato in HM20 and HM20-T embedding methods.

(E) Enlarged images from (D).

(F) Fluorescence intensity plots for the lines labeled in (e1) and (e2).

(G) Fine structures were well embedded in the HM20-T method. (g1) and (g2) Enlarged images from (G).

(H) Quantitative analysis of fluorescence preservation of tdTomato before and after embedding (n = 14 independent experiments for HM20 method; n = 9 independent experiments for HM20-T). Data presented as mean ± SEM. Statistical analysis was performed by unpaired t-test, ****$p < 0.0001$. Raw data were shown in Tables S3–S6. Scale bars: (A, E, and G) 5 μm; (D) 20 μm.

of mice (Figure S1A). The enlarged view showed that the cell body, axons, and dendrites of a single neuron could be observed (Figure S1B). We labeled PV neurons in basal forebrain by mRuby protein. After embedding, both neurons and axons could be clearly obtained by the imaging system (Figure S1C). The fluorescence preservation rate of YFP was 86.44 ± 3.11%, and mRuby was 82.23 ± 2.81% (Figure S1D). These results indicated that HM20-T is suitable for a variety of commonly used fluorescent proteins.

The HM20-T method was compatible with fluorescent dyes or probes

Fluorescent dyes or probes are also widely used when labeling various biological tissues. To test whether the HM20-T method could preserve fine structures labeled with fluorescent dyes or fluorescent probes, we embedded brain samples with multiple fluorescent dyes or fluorescent probes, such as DyLight 488 conjugated lycopersicon esculentum lectin (LEL-DyLight 488), DANIR-8C, and Fluoro-Gold. LEL-DyLight 488 labeled blood vessels by tail vein labeling, DANIR-8C labeled amyloid-β plaque in five familial Alzheimer's disease mutations mice (5×FAD), and Fluoro-Gold labeled input neurons (Figures 4A and 4B). We

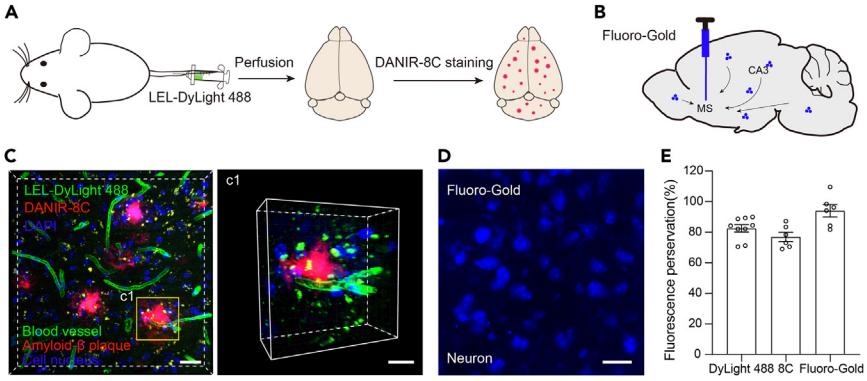

Figure 4. HM20-T was compatible with multiple fluorescent dyes or fluorescent probes

(A) Flow chart of vascular labeling and amyloid-β plaque staining.

(B) Schematic diagram of injection Fluoro-Gold.

(C) The three-dimensional image of the amyloid-β around blood vessel. (c1) Enlarged image from (C).

(D) Fluoro-Gold signals after embedding.

(E) The preservation ratio of fluorescent dyes and probes after embedding (n = 9 independent experiments for LEL-DyLight 488; n = 6 independent experiments for DANIR-8C; n = 6 independent experiments for Fluoro-Gold). Data presented as mean ± SEM. Raw data were shown in Table S7. Scale bars: (C, D) 20 μm; (c1) 10 μm.

observed that the amyloid-β in close proximity to blood vessel (Figure 4C). After embedding, input neurons labeled by Fluoro-Gold can be clearly indentified (Figure 4D). As shown in Figure 4E and Table S7, the fluorescence preservation rates of LEL-DyLight 488, DANIR-8C, and Fluoro-Gold were 82.55 ± 2.41%, 76.93 ± 2.99%, and 94.06 ± 4.12%, respectively. Simultaneous acquisition of blood vessels, amyloid-β plaque, and neurons was beneficial for studying their interactions in Alzheimer's disease. These data confirmed that the HM20-T method was suitable for simultaneous acquisition of fluorescent protein and fluorescent dyes or probes.

Acquisition of the long-rang projection axons and boutons in the whole brain

To demonstrate HM20-T resin method imaging quality in the whole brain, we injected AAV sparsely labeled virus in the basal forebrain of PV-ires-cre transgenic mice. Here, we selected the anterior and medial part of the basal forebrain, the medial septum nucleus (MS) and the diagonal band nucleus (VDB), which participated in complex functions through abundant connections with the downstream areas. We acquired the axon projection in the whole brain. As shown in Figure 5A, we found that axon projections of MS/VDB were distributed in hippocampal region (HIP) and retrohippocampal region (RHP). By zooming in MS, CA1, and CA3, we clearly observed axon structures near the injection site and distal terminals, such as boutons. These results indicated that the quality of fluorescent signals was stable during whole-brain imaging. Furthermore, axons and terminals in presubiculum (PRE) were clearly discernible in three dimensions (3D) (Figure 5B). As shown in Figures 5C and 5D, our results showed that we could trace the axon with brighter fluorescence to weak terminals signals and indicated that axons and terminals of different levels could be well preservation and reconstructed. Quantitative analysis of axon gray values of different segments demonstrated that HM20-T could obtain fluorescent information in multi-level branches (Figure 5E and Table S8). At the same time, swollen axon terminals revealed that full morphology and precise structure of neurons were preserved in HM20-T method. In summary, HM20-T method provided a powerful tool for neuronal reconstruction and neural circuit analysis.

Immunoreactivity was retained in the HM20-T resin embedding method

Low-temperature facilitated preservation of immunoreactivity of biological samples. To determine if biological tissues remained immunoreactive after resin embedding, we tested antibodies for immunoreactivity. Thy1-GFP samples were slice to 10 μm semi-thin sections by fMOST system and we incubated sections with antibody directed against GFP (Figure 6A). After staining with anti-GFP antibodies, immunofluorescent signals accumulated in soma and axon. In addition, tubulin is a cytoskeletal protein involved in cell movement, material transport, and other activities, mainly composed of alpha-Tubulin and beta-Tubulin. Beta III-Tubulin mainly existed in neurons and was one of the neuronal markers. We observed that the

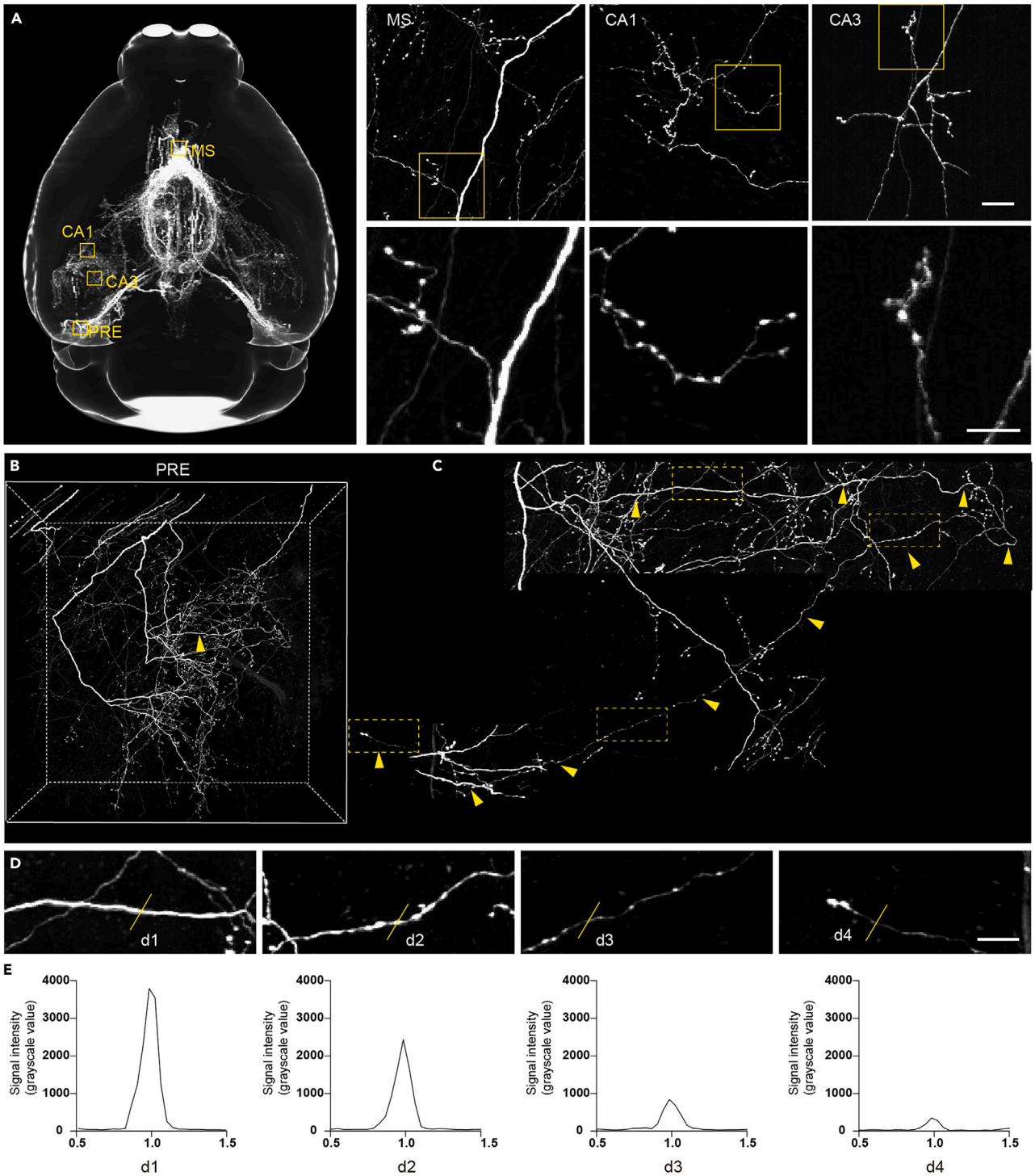

Figure 5. Axon projection pattern of PV neurons after 3D reconstruction in the whole brain

(A) Long projection axon terminals from basal forebrain.

(B) 3D view of all the axon reconstruction in PRE.

(C) Projection distribution of a single axon in B (yellow arrows represent axon direction).

(D) Cropped image of the axon in (C).

(E) Signal intensity along the white lines in the (D). Medial septum, MS; Field CA1, CA1; Field CA3, CA3. Raw data were shown in Table S8. Scale bars: (A) up, 20 μm; down, 10 μm; (D) 10 μm.

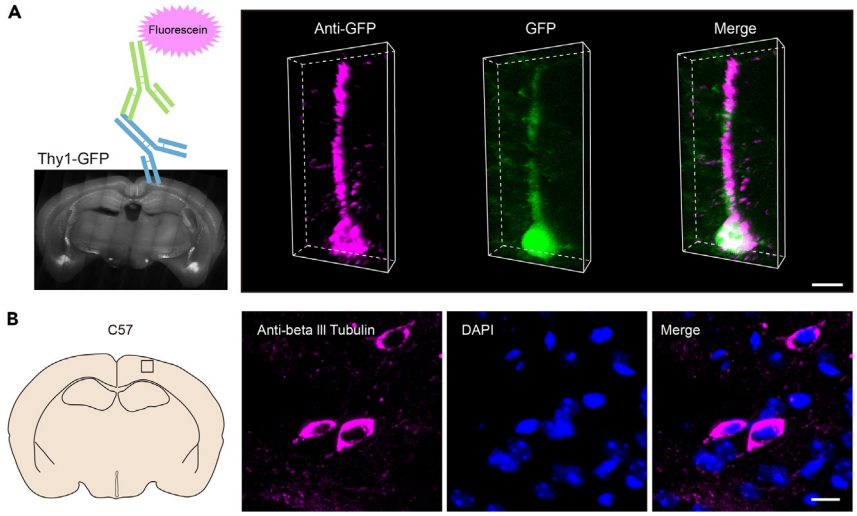

Figure 6. Preservation of immunoreactivity of biological tissues using HM20-T method

(A) GFP immunofluorescence in the cerebral cortex of a Thy1-GFP mouse.

(B) Immunochemical staining of beta III tubulin after embedding. Scale bars: (A, B) 10 μm.

immunofluorescence of beta III-Tubulin co-localized with DAPI (Figure 6B). The specificity of immunochemical staining by GFP and beta III-Tubulin demonstrated that proteins retained immunoreactivity after resin embedding. HM20-T method was expected to be used for the identification of molecular phenotypes for samples using fMOST system imaging in the future.

DISCUSSION

In this study, we developed an HM20-T resin embedding method for the acquisition of fluorescent signals of precise structures. To acquire precise structure information in large-volume sample and maintain their fluorescent signals, we modified the resin embedding methods to avoid signal quenching by reducing the polymerization temperature. In this study, we found polymerization temperature of 4°C or −20°C were suitable for fluorescent preservation of precise structures. Normally, low-temperature polymerization mainly could be achieved in two ways. One way is UV polymerization, which has poor penetration ability for thick tissue.[25] The other way is catalytic polymerization of redox reaction, which only needs lower activation energy to initiate reaction polymerization. However, the catalytic polymerization method had not yet been performed on large-volume samples because of the difficulty of uniform polymerization in deep tissue. In previous reports, BPO and DMA were used as initiators and accelerators. DMT was more active and hence more suitable for low-temperature environment than DMA.[26] Here, we added DMT as a new polymerization accelerator for embedding at −20°C. After extensive testing, we found that 0.6% BPO and 0.7% DMT were the optimal concentration combination. The success ratio of whole-brain resin embedding was over 98%, which meant that large-volume samples can be stably polymerized at low temperatures. It plays an important role in large-scale sample preparation and acquisition of sample information. Moreover, the HM20-T method established in this study is similar to the HM20 method, such as hardness, embedding time, and cutting thickness (Table 3). During the whole-brain imaging, the HM20-T resin method can be stably sliced and imaged in an aqueous environment. This method was more applicable to imaging precise structures labeled by various fluorescent proteins or probes and could be used for the identification of molecular phenotypes after imaging in the future.

The HM20-T embedding method was compatible with various fine structures labeled by fluorescent protein and dyes. EGFP labeled presynaptic elements structures could be clearly observed after HM20-T resin embedding. Fluorescence preservation and number preservation of presynaptic elements were doubled (Figures 3A–3C). The HM20-T method maintained the fluorescence of boutons labeled by tdTomato and low background fluorescence for detection of weak signals in large-volume samples. Moreover, the HM20-T method was also compatible with fluorescent dyes and probes, including LEL-DyLight 488, DANIR-8C, and Fluoro-Gold. Last, this method might not be limited to fluorescent protein or probes

Table 3. Detailed parameter comparison between HM20 method and HM20-T method

Method	Hardness	Embedding time (dehydration/ penetration/polymerization)	Cutting thickness	Fluorescent protein/probe	Immunochemical staining
HM20	80 HD	10 h/51 h/20 h	1 μm	YFP/GFP	—
HM20-T	86 HD	10 h/51 h/48 h	1 μm	YFP/GFP/tdTomato/mRuby/ LEL-DyLight488/DANIR-8C/ Fluoro-Gold	Compatibility

used in this study. There are improved fluorescent proteins with higher fluorescence brightness and stability, such as mGreenLantern, mClover3, mNeonGreen, mRuby3, mTagBFP2, and hfYFP.[27–29] They have similar excitation properties to conventional fluorescent proteins, such as YFP and mRuby. We think that HM20-T method is not limited to the fluorescent proteins described in this paper, but also applicable to some improved fluorescent proteins. In the future, we will perform further experiments to verify this.

In addition, the low-temperature resin embedding method preserved antigenic determinants of biological tissues and was suitable for immunochemical staining after imaging. Immunochemical staining of tubulin and GFP demonstrated that HM20-T retained immunoreactivity of brain samples, but the results were not as satisfactory as immunostained fresh brain slices. The reason might be that the HM20 resin was a hydrophobic resin and the crosslinking was relatively dense so antibody penetration was hindered. In the future, we could add other reagents to unravel resin crosslink before immunochemical staining.

In summary, to simultaneous acquire multiple fluorescent labeled samples with precise structures, we added a new accelerator and selected the optimal concentration during the plastic resin embedding process. After resin embedding, the precise structures labeled with fluorescent proteins and fluorescent dyes could be retained using the HM20-T method. In conclusion, the HM20-T resin embedding method could be used for various fine structures imaging, which might facilitate our understanding of complex structures and functions of neural circuits.

Limitations of the study

In the present study, we developed the low-temperature resin embedding method suitable for various precise structures. However, the current limitation of the study is that the HM20-T method is not used to test different animal models, such as tree shrew, marmoset, and macaque. In the future, we need to determine whether the HM20-T method is applicable to non-human brain. These studies contribute to understanding of the structure and function of the human brain and treating various neurological diseases.

STAR★METHODS

Detailed methods are provided in the online version of this paper and include the following:

- KEY RESOURCES TABLE
- RESOURCE AVAILABILITY
  - Lead contact
  - Materials availaility
  - Data and code availability
- EXPERIMENTAL MODEL AND SUBJECT DETAILS
  - Animals
- METHOD DETAILS
  - Stereotactic injection of virus
  - Vasculature labeling
  - Amyloid-β plaque staining
  - Tissue preparation
  - Resin embedding
- QUANTIFICATION AND STATISTICAL ANALYSIS
  - Fluorescence intensity quantitative analysis
  - Statistics analysis

SUPPLEMENTAL INFORMATION

Supplemental information can be found online at https://doi.org/10.1016/j.isci.2023.106705.

ACKNOWLEDGMENTS

The authors thank Die Hu, for help with experiments and data analysis. We also thank Jing Yuan, Anan Li for help with whole-brain imaging and data analysis. This work was financially supported by the STI2030-Major Projects (No. 2021ZD0201001, 2021ZD0201000), National Nature Science Foundation of China (Nos. 32192412 and 31871088) and CAMS Innovation Fund for Medical Sciences 2019-I2M-5-014. We thank the Optical Bioimaging Core Facility of HUST for technical assistance.

AUTHOR CONTRIBUTIONS

X.L. and H.G. conceived and designed the study. J.T. optimized resin embedding and analyzed the data. Y.C. performed the virus injections. T.J. and X.J. performed the whole brain imaging and data processing. J.T., X.L., and H.G. wrote and modified the manuscript.

DECLARATION OF INTERESTS

The authors declare no competing interests.

INCLUSION AND DIVERSITY

We support inclusive, diverse, and equitable conduct of research.

Received: December 23, 2022
Revised: March 3, 2023
Accepted: April 17, 2023
Published: April 20, 2023

REFERENCES

1. Xu, W., and Südhof, T.C. (2013). A neural circuit for memory specificity and generalization. Science *339*, 1290–1295. https://doi.org/10.1126/science.1229534.

2. Tian, J., Ren, M., Zhao, P., Luo, S., Chen, Y., Xu, X., Jiang, T., Sun, Q., Li, A., Gong, H., et al. (2022). Dissection of the long-range projections of specific neurons at the synaptic level in the whole mouse brain. Proc. Natl. Acad. Sci. USA *119*. e2202536119. https://doi.org/10.1073/pnas.2202536119.

3. Oh, S.W., Harris, J.A., Ng, L., Winslow, B., Cain, N., Mihalas, S., Wang, Q., Lau, C., Kuan, L., Henry, A.M., et al. (2014). A mesoscale connectome of the mouse brain. Nature *508*, 207–214. https://doi.org/10.1038/nature13186.

4. Wall, N.R., Wickersham, I.R., Cetin, A., De La Parra, M., and Callaway, E.M. (2010). Monosynaptic circuit tracing in vivo through Cre-dependent targeting and complementation of modified rabies virus. Proc. Natl. Acad. Sci. USA *107*, 21848–21853. https://doi.org/10.1073/pnas.1011756107.

5. Sun, Q., Li, X., Ren, M., Zhao, M., Zhong, Q., Ren, Y., Luo, P., Ni, H., Zhang, X., Zhang, C., et al. (2019). A whole-brain map of long-range inputs to GABAergic interneurons in the mouse medial prefrontal cortex. Nat. Neurosci. *22*, 1357–1370. https://doi.org/10.1038/s41593-019-0429-9.

6. Zhou, C., Yang, X., Wu, S., Zhong, Q., Luo, T., Li, A., Liu, G., Sun, Q., Luo, P., Deng, L., et al. (2022). Continuous subcellular resolution three-dimensional imaging on intact macaque brain. Sci. Bull. *67*, 85–96. https://doi.org/10.1016/j.scib.2021.08.003.

7. Sotoudeh, N., Namavar, M.R., Bagheri, F., and Zarifkar, A. (2022). The medial prefrontal cortex to the medial amygdala connections may affect the anxiety level in aged rats. Brain Behav. *12*, e2616. https://doi.org/10.1002/brb3.2616.

8. Unal, G., Joshi, A., Viney, T.J., Kis, V., and Somogyi, P. (2015). Synaptic targets of medial septal projections in the hippocampus and extrahippocampal cortices of the mouse. J. Neurosci. *35*, 15812–15826. https://doi.org/10.1523/jneurosci.2639-15.2015.

9. Nishimura, W., Sakaue-Sawano, A., Takahashi, S., Miyawaki, A., Yasuda, K., and Noda, Y. (2018). Optical clearing of the pancreas for visualization of mature β-cells and vessels in mice. Islets *10*, e1451282. https://doi.org/10.1080/19382014.2018.1451282.

10. Giannoni, P., Arango-Lievano, M., Neves, I.D., Rousset, M.C., Baranger, K., Rivera, S., Jeanneteau, F., Claeysen, S., and Marchi, N. (2016). Cerebrovascular pathology during the progression of experimental Alzheimer's disease. Neurobiol. Dis. *88*, 107–117. https://doi.org/10.1016/j.nbd.2016.01.001.

11. Zhang, J., Long, B., Li, A., Sun, Q., Tian, J., Luo, T., Ding, Z., Gong, H., and Li, X. (2020). Whole-brain three-dimensional profiling reveals brain region specific axon vulnerability in 5xFAD mouse model. Front. Neuroanat. *14*, 608177. https://doi.org/10.3389/fnana.2020.608177.

12. Gong, H., Xu, D., Yuan, J., Li, X., Guo, C., Peng, J., Li, Y., Schwarz, L.A., Li, A., Hu, B., et al. (2016). High-throughput dual-colour precision imaging for brain-wide connectome with cytoarchitectonic landmarks at the cellular level. Nat. Commun. *7*, 12142. https://doi.org/10.1038/ncomms12142.

13. Luo, T., Deng, L., Li, A., Zhou, C., Shao, S., Sun, Q., Gong, H., Yang, X., and Li, X. (2020). Scalable resin embedding method for large-volume brain tissues with high fluorescence preservation capacity. iScience *23*, 101717. https://doi.org/10.1016/j.isci.2020.101717.

14. Wang, X., Xiong, H., Liu, Y., Yang, T., Li, A., Huang, F., Yin, F., Su, L., Liu, L., Li, N., et al. (2021). Chemical sectioning fluorescence tomography: high-throughput, high-contrast, multicolor, whole-brain imaging at subcellular resolution. Cell Rep. *34*, 108709. https://doi.org/10.1016/j.celrep.2021.108709.

15. Zhong, Q., Li, A., Jin, R., Zhang, D., Li, X., Jia, X., Ding, Z., Luo, P., Zhou, C., Jiang, C., et al. (2021). High-definition imaging using line-illumination modulation microscopy. Nat. Methods *18*, 309–315. https://doi.org/10.1038/s41592-021-01074-x.

16. Gang, Y., Zhou, H., Jia, Y., Liu, L., Liu, X., Rao, G., Li, L., Wang, X., Lv, X., Xiong, H., et al. (2017). Embedding and chemical reactivation of green fluorescent protein in the whole mouse brain for optical micro-imaging. Front. Neurosci. *11*, 121. https://doi.org/10.3389/fnins.2017.00121.

17. Ren, M., Tian, J., Zhao, P., Luo, J., Feng, Z., Gong, H., and Li, X. (2018). Simultaneous acquisition of multicolor information from neural circuits in resin-embedded samples. Front. Neurosci. *12*, 885. https://doi.org/10.3389/fnins.2018.00885.

18. Zhang, C., Liu, M.S., and Xing, X.H. (2009). Temperature influence on fluorescence intensity and enzyme activity of the fusion protein of GFP and hyperthermophilic xylanase. Appl. Microbiol. Biotechnol. *84*, 511–517. https://doi.org/10.1007/s00253-009-2006-8.

19. Gerrits, P.O., and Horobin, R.W. (1996). Glycol methacrylate embedding for light microscopy: basic principles and trouble-shooting. J. Histotechnol. *19*, 297–311. https://doi.org/10.1179/his.1996.19.4.297.

20. Zhang, Q., Wang, J., Wu, H., Zhang, L., Zhou, J., Ye, Q., Shao, X., Guan, C., Xu, J., Yang, Y., et al. (2010). Low-temperature glycol methacrylate resin embedding method: a protocol suitable for bone marrow immunohistochemistry, PCR, and fish analysis. Microsc. Res. Tech. *73*, 1067–1071. https://doi.org/10.1002/jemt.20836.

21. Wolf, E., Röser, K., Hahn, M., Welkerling, H., and Delling, G. (1992). Enzyme and immunohistochemistry on undecalcified bone and bone marrow biopsies after embedding in plastic: a new embedding method for routine application. Virchows Arch. *420*, 17–24. https://doi.org/10.1007/BF01605979.

22. Quester, R., Knifka, J., and Schröder, R. (2002). Optimization of glycol methacrylate embedding of large specimens in neurological research. Study of rat skull-brain specimens after implantation of polyester meshes. J. Neurosci. Methods *113*, 15–26. https://doi.org/10.1016/s0165-0270(01)00469-1.

23. Hatada, K., Kitayama, T., and Masuda, E. (1986). Studies on the radical polymerization of methyl methacrylate in bulk and in benzene using totally deuterated monomer technique. Polym. J. *18*, 395–402. https://doi.org/10.1295/polymj.18.395.

24. Qiu, K., Zhang, J., and Feng, X. (1981). Studies on vinyl polymerization with initiation system containing amine derivatives. Chin. J. Polym. Sci. *1*.

25. Newman, G.R., and Hobot, J.A. (1999). Resins for combined light and electron microscopy: a half century of development. Histochem. J. *31*, 495–505. https://doi.org/10.1023/a:1003850921869.

26. Liu, X., Yao, Z., Xue, W., and Li, X. (2019). Effect of temperature and accelerator on gel time and compressive strength of resin anchoring agent. Adv. Polym. Technol. *2019*, 1–11. https://doi.org/10.1155/2019/3546153.

27. Bajar, B.T., Wang, E.S., Lam, A.J., Kim, B.B., Jacobs, C.L., Howe, E.S., Davidson, M.W., Lin, M.Z., and Chu, J. (2016). Improving brightness and photostability of green and red fluorescent proteins for live cell imaging and FRET reporting. Sci. Rep. *6*, 20889. https://doi.org/10.1038/srep20889.

28. Campbell, B.C., Nabel, E.M., Murdock, M.H., Lao-Peregrin, C., Tsoulfas, P., Blackmore, M.G., Lee, F.S., Liston, C., Morishita, H., and Petsko, G.A. (2020). mGreenLantern: a bright monomeric fluorescent protein with rapid expression and cell filling properties for neuronal imaging. Proc. Natl. Acad. Sci. USA *117*, 30710–30721. https://doi.org/10.1073/pnas.2000942117.

29. Subach, O.M., Cranfill, P.J., Davidson, M.W., and Verkhusha, V.V. (2011). An enhanced monomeric blue fluorescent protein with the high chemical stability of the chromophore. PLoS One *6*, e28674. https://doi.org/10.1371/journal.pone.0028674.

STAR★METHODS

KEY RESOURCES TABLE

REAGENT or RESOURCE	SOURCE	IDENTIFIER
Antibodies		
GFP	abcam	Cat#ab290
Beta III Tubulin	abcam	Cat#ab78078
647 donkey anti Rabbit	Invitrogen	Cat#A31573
647 donkey anti Mouse	Invitrogen	Cat#A31571
Bacterial and virus strains		
AAV2/9-hSyn-flex-tdTomato-T2A-synaptophysin-EGFP-WPRE-pA	Shanghai Taitool Bioscience Co., Ltd	Cat#S0250
Fluoro-Gold	Biotium	Cat#80023
Chemicals, peptides, and recombinant proteins		
HM20	Electron Microscopy Science	Cat#14340
PBS	Sigma-Aldrich	Cat#P3813
PFA	Sigma-Aldrich	Cat#P6148
DMT	aladdin	Cat#N158974
BPO	Electron Microscopy Science	Cat#18181
AIBN	Shanghai Shisi Hewei Chemical Co., Ltd	Cat#214-2013
LEL-DyLight 488	Vectro laboratories	Cat#DL-1174-1
DAPI	ThermoFisher	Cat#D1306
Software and algorithms		
FIJI	Open Source Software ImageJ	https://imagej.nih.gov/ij/
GraphPad Prism 6.01	GraphPad	https://www.graphpad.com/

RESOURCE AVAILABILITY

Lead contact

Further information and requests for resources and reagents should be directed to and will be fulfilled by the lead contact, Xiangning Li (lixiangning@mail.hust.edu.cn).

Materials availaility

This study did not generate new unique reagents or materials.

Data and code availability

- The datasets and images generated during this study are available from the lead contact upon request.
- This paper does not report original code.
- Any additional information required to reanalyze the data reported in this paper is available from the lead contact upon request.

EXPERIMENTAL MODEL AND SUBJECT DETAILS

Animals

All animal experiments were approved by the Animal Ethics Committee of Huazhong University of Science and Technology. Transgenic animals, expressing Cre under the control of cell-type specific promoters, mice were purchased from Jackson Laboratory. Transgenic animals included 2–3 months male Thy1-GFP, Thy1-YFP, PV-ires-cre, 5xFAD-cre, VIP-ires-cre, and Ai14 mice. Two-monthold male C57BL/6J mice

were purchased from Beijing Huafukang Biotechnology Co., Ltd. VIP-ires-cre; Ai14 were generated by crossing VIP-ires-cre and Ai14 mice.

METHOD DETAILS

Stereotactic injection of virus

Anterograde tracing was performed using adeno-associated virus (AAV). For polymerization temperature test, 100 nL AAV2/9-hSyn-flex-tdTomato-T2A-synaptophysin-EGFP-WPRE-pA (1×10^{12} genome copies mL^{-1}) was injected into the MS/VDB at AP: 0.98 mm, ML: 0 mm, DV: −4.8 mm. AAV2/9-hSyn-flex-tdTomato-T2A-synaptophysin-EGFP-WPRE-pA purchased from Shanghai Taitool Bioscience Co., Ltd.

Vasculature labeling

C57BL/6J were anesthetized and injected 0.1 mL LEL-DyLight 488 via the caudal vein. LEL-DyLight 488 was diluted in 0.01 mol/L PBS buffer to a concentration of 20 μg/mL. After injection, the mice were placed in a warm environment for 30 minutes to perfusion.

Amyloid-β plaque staining

The staining method refer to previous studies. Donor-acceptor near-infrared 8C (DANIR-8C) was a gift from Beijing Normal University. The whole staining process including four days: 15% solution for 24 h, 30% solution for 48 h, and 0% solution for 24 h, and 70% ethanol for 6 h in 4°C dark environment. The 15% solution includes 15% sucrose (wt/vol), 0.01 mol/mL DANIR-8C, 0.1% Triton X-100, and 0.05% sodium azide; The 15% solution includes 30% sucrose (wt/vol), 0.01 mol/mL DANIR-8C, 0.1% Triton X-100, and 0.05% sodium azide; The 0% solution includes 0% sucrose (wt/vol), 0.01 mol/mL DANIR-8C, 0.1% Triton X-100, and 0.05% sodium azide.

Tissue preparation

All animals were anesthesia with a 1% solution of sodium pentobarbital and 3% solution of ethyl carbamate and transcranial perfused with ice-cold 0.01 mol/L PBS (Sigma-Aldrich, cat. no. P3813), then freshly prepared, ice-cold 4% paraformaldehyde (Sigma-Aldrich, cat. no. P6148) in 0.01 mol/L PBS. All samples were excised and post-fixed with ice-cold 4% paraformaldehyde for 24 h and then sliced into 50 μm or 100 μm with a vibratome.

Resin embedding

We used 100 μm coronal plane brain slices to compare the resin embedding method before and after optimization. Firstly, these slices were dehydrated in a graded ethanol series (50%, 75%, 95%, and 100%, each step 5 min at 4°C). Secondly, these slices were penetration in a graded HM20 resin series (50%, 75%, 100% HM20 resin, each step 5 min at 4°C) and 100% HM20 for 6 h at 4°C. Lastly, some slices were polymerized by gradient temperature in a vacuum environment, and the polymerization temperature was 38°C for 12 h, 45°C for 8 h, and 45°C for 12 h. And other slices were embedded in polymerization solution containing 0.7% DMT (N, N-Dimethyl-*p*-toluidine) at −20°C for 24 h. For whole-brain embedding, the brains were dehydrated in a graded ethanol series (50%, 75%, 95%, 100%, each step 1 h at 4°C) and were penetration in a graded resin series (50%, 75%, 100% HM20 resin, each step 2 h at 4°C). Lastly, the samples were penetration in 100% HM20 solution for 48 h at 4°C, and embedded in 100% HM20 with 0.7% DMT at −20°C for 48 h. The 100% HM20 solution of the optimized method includes 62.3 g monomer, 14.9 g crosslinker, and 0.6 g BPO (Benzoyl peroxide). The 50% and 75% HM20 (wt/wt) were prepared from ethanol and HM20. The 100% HM20 solution of theold method includes 82.5 g monomer, 17.5 g crosslinker, and 0.16 g AIBN.

QUANTIFICATION AND STATISTICAL ANALYSIS

Fluorescence intensity quantitative analysis

We imaged the brain slices in the same region before and after embedding with the same parameters, which did not overburden the fluorescent signal. The fluorescence intensity of fluorescence proteins or fluorescent dyes were read out by FIJI software. We used the oval tool to read out the mean gray value of signals before and after embedding. The fluorescence preservation ratio = $I/I_0\times100\%$ (I: the mean gray value before embedding; I_0: the mean gray value after embedding). Multiple independent samples were used for statistical analysis.

Statistics analysis

GraphPad Prism 6.01 was used for statistical analysis. And for all statistical analysis data, significance was represented as *$p \leq 0.05$, **$p \leq 0.01$, ***$p \leq 0.001$, and ****$p \leq 0.0001$. The unpaired t-test performed using GraphPad Prism 6.01. And all results were presented as the mean $\pm$ SEM.